

# Efficient computational algorithm for stress analysis in hydro-sediment-morphodynamic models

Alia Al-Ghosoun, Ashraf S Osman, and Mohammed Seaid

Department of Engineering, University of Durham, South Road, Durham DH1 3LE,  
United Kingdom

**Abstract.** Understanding of complex stress distributions in lake beds and river embankments is crucial in many designs in civil and geotechnical engineering. We propose an accurate and efficient computational algorithm for stress analysis in hydro-sediment-morphodynamic models. The governing equations consist of the linear elasticity in the bed topography coupled to the shallow water hydro-sediment-morphodynamic equations. Transfer conditions at the bed interface between the water surface and the bedload are also developed using frictional forces and hydrostatic pressures. A hybrid finite volume/finite element method is implemented for the numerical solution of the proposed model. Well-balanced discretization of the gradient fluxes and source terms is formulated for the finite volume and the treatment of dry areas in the model is discussed in the present study. The finite element method uses quadratic elements on unstructured meshes and interfacial forces are samples on the common nodes for finite volume and finite element grids. Numerical results are presented for a dam-break problem in hydro-sediment-morphodynamic models and the computed solutions demonstrated the ability of the proposed model in accurately capturing the stress distributions for erosional and depositional deformations. In addition, the coupled model is accurate, very efficient, well-balanced and it can solve complex geometries.

**Keywords:** Stress analysis · Finite element method · Finite volume method · Shallow water flows · Sediment transport · Morphodynamics.

## 1 Introduction

Water movement over an erodible bed in either steady or unsteady conditions can scour particles off the bed and transport them some distance [13]. These particles can either travel as suspended sediment which is immersed in the flow of water itself or as bedload, where sediment tumbles across of the bed [10]. Understanding the dynamics of sediment transport and erosion-deposition processes is important in different applications like road cuts, embankments and dams designs [6]. Erosion and deposition of soil comprise one of the major concerns in studying soil properties. Spacial and temporal informations of soil erosion processes is required to reflect the pattern of sediment transport during

different environmental conditions [14]. Indeed, previous knowledge of the factors affecting soil erosion is very useful in different morphodynamic applications like dam-break, dam removal and storms [1]. In recent years, the investigations of soil erosion and deposition through the development of different algorithms have been rapidly increased [16]. These algorithms depend on different equations, some of them depends on the fundamental energy transport equations [5], sediment flux equation [9] and the steady-state continuity equations for deposition [12]. However, there are still many models and techniques which suffer from a range of problems, such as over-estimation due to parameters in compliance with the initial conditions and the assumptions unsuitability to the present case alongside with the existence of uncertainty in the system parameters [15].

Sediment is continually subjected to physical stress in the environment. These stresses are of paramount importance to geomorphologists because they are a driver of geomorphic change. These stresses can describe forces applied to the soil, that result in sediment deformation or fracture [7]. Many excellent methods have been developed to quantify these stresses in soil. The most accurate of these are conducted within the laboratory using specialist equipment. However, cohesive sediment undergoes significant changes in sediment properties when it is cored, transported, stored and finally analysed in the laboratory, and these changes can significantly alter its shear strength [11]. Different techniques have been using to quantify the stresses in soil. In the current study, a coupled finite element/finite volume method for solving soil stresses over erodible beds is proposed. The governing equations consist of the one-dimensional non-linear shallow water equations for the water flow and a two-dimensional linear elasticity model for the bed deformation. Deformations in the topography can be caused as a result of the hydrostatic pressure distribution and the frictional force obtained from the shallow water movement. Coupling conditions at the interface are also investigated in this study and a well-balanced finite volume method using non-uniform grids is implemented without the requirements of the interpolation procedures at the interface between the finite element and finite volume nodes. On the other hand, a force is sampled from the hydrostatic pressure and applied on the bed surface to be used in the stress analysis. Numerical results for both the bed-load and stress distributions are presented in this study for a dam-break problem over erodible bed.

This paper is organized as follows. In section 2 we present the governing equations used for the hydro-sediment-morphodynamic models. Section 3 is devoted to the development of an efficient computational algorithm for solving the coupled system. We formulate the hybrid finite element method/finite volume method. In this section we also discuss the coupling conditions at the interface. In section 4, we examine the numerical performance of the proposed method using several examples of hydro-sediment-morphodynamic problems. Our new approach is demonstrated to enjoy the expected efficiency as well as the accuracy. Concluding remarks are summarized in section 5.

## 2 Equations for hydro-sediment-morphodynamic models

In the present study, we assume a longitudinal one-dimensional shallow water-sediment flow over an erodible bed composed of uniform, non-cohesive sediment of particle diameter  $d_s$ . Therefore, the governing shallow water hydro-sediment-morphodynamic equations can be derived by directly applying the Reynolds transport theorem in fluid dynamics assuming a hydrostatic pressure and the flow is almost horizontal with the vertical component of the acceleration is vanishingly small. The model consists of mass and momentum conservation laws for the water-sediment mixture and separate mass conservation laws for sediment and bed material. The resulting system of equations can be expressed in the standard well-structured conservation form as

$$\frac{\partial \mathbf{q}}{\partial t} + \frac{\partial \mathbf{F}(\mathbf{q})}{\partial x} = \mathbf{Q}(\mathbf{q}) + \mathbf{S}(\mathbf{q}), \quad (1)$$

where the vector of unknowns  $\mathbf{q}$  and the flux vector  $\mathbf{F}(\mathbf{q})$  are

$$\mathbf{q} = \begin{pmatrix} h \\ hv \\ hc \\ Z \end{pmatrix}, \quad \mathbf{F}(\mathbf{q}) = \begin{pmatrix} hv \\ hv^2 + \frac{1}{2}gh^2 \\ hvc \\ \frac{q_b}{1-p} \end{pmatrix},$$

and the source vector  $\mathbf{S}(\mathbf{q})$  is

$$\mathbf{S}(\mathbf{q}) = \begin{pmatrix} \frac{\mathcal{E} - \mathcal{D}}{1-p} \\ -\frac{(\rho_0 - \rho)(\mathcal{E} - \mathcal{D})v}{\rho(1-p)} - gh \frac{n_b^2 v |v|}{h^{4/3}} \\ \frac{\mathcal{E} - \mathcal{D}}{\mathcal{E} - \mathcal{D}} \\ -\frac{\mathcal{E} - \mathcal{D}}{1-p} \end{pmatrix}.$$

The differential source term  $\mathbf{Q}(\mathbf{q})$  is defined as

$$\mathbf{Q}(\mathbf{q}) = \begin{pmatrix} 0 \\ -gh \frac{\partial Z}{\partial x} - \frac{(\rho_s - \rho_w)}{2\rho} gh^2 \frac{\partial c}{\partial x} \\ 0 \\ 0 \end{pmatrix}.$$

Here,  $v$  is the depth-averaged water velocity,  $h$  the water depth,  $Z$  the bottom topography,  $g$  the gravitational acceleration,  $p$  the porosity,  $\rho_w$  the water density,  $\rho_s$  the sediment density,  $c$  is the depth-averaged concentration of the suspended sediment,  $n_b$  is the Manning roughness coefficient,  $\mathcal{E}$  and  $\mathcal{D}$  represent

the entrainment and deposition terms in upward and downward directions, respectively. The density of the water-sediment mixture  $\rho$  and the density of the saturated bed  $\rho_0$  are defined by

$$\rho = \rho_w(1 - c) + \rho_s c, \quad \rho_0 = \rho_w p + \rho_s(1 - p). \quad (2)$$

It should be noted that although there are various bedload transport formulae which were empirically proposed based on laboratory or fieldwork datasets, none can be universally applied due to the range and varying distribution of grain sizes. In this study, we consider the Grass formula [8]

$$q_b = A_g v^3, \quad (3)$$

where  $A_g \in [0, 1]$  is a dimensionless constant usually obtained experimentally by accounting for the diameter of the particles and the kinematic viscosity. For values of  $A_g$  close to zero, the model shows a weak interaction between the sediment bottom and the fluid. However, for values of  $A_g$  close to one, the interaction between the sediment bottom and the fluid is strong.

To determine the entrainment and deposition terms in the above equations we assume a non-cohesive sediment and we use empirical relations reported in [4]. Thus,

$$D = w \alpha_c (1 - \alpha_c c)^m c, \quad (4)$$

where  $w$  is the settling velocity of a single particle in tranquil water

$$\omega = \sqrt{\left(\frac{13.95\nu}{d}\right)^2 + 1.09sgd} - \frac{13.95\nu}{d}, \quad (5)$$

with  $\nu$  is the kinematic viscosity of the water,  $d$  the averaged diameter of the sediment particle,  $m$  an exponent indicating the effects of hindered settling due to high sediment concentrations and it is computed using the Reynolds number of the particle as

$$m = 4.45Re^{-0.1}, \quad Re = \frac{wd}{\nu}.$$

To ensure that the near-bed concentration does not exceed  $(1 - p)$ , the coefficient  $\alpha_c$  is computed by [4]

$$\alpha_c = \min\left(2, \frac{1 - p}{c}\right).$$

For the entrainment of a cohesive material, the following relation is used

$$E = \begin{cases} \varphi \frac{\theta - \theta_c}{h} v d^{-0.2}, & \text{if } \theta \geq \theta_c, \\ 0, & \text{otherwise,} \end{cases} \quad (6)$$

where  $\varphi$  is a coefficient to control the erosion forces determined by

$$\varphi = \varphi_c \frac{560(1 - p)\nu^{0.8}}{3(sg)^{0.4}\theta_c},$$

with  $\varphi_c$  is a dimensionless value that depends on the phenomenon to recreate. Here,  $\theta_c$  is a critical value of Shields parameter for the initiation of the sediment motion and  $\theta$  is the Shields coefficient defined by

$$\theta = \frac{u_*^2}{sgd}, \quad (7)$$

with  $u_*$  is the friction velocity defined as

$$u_* = \sqrt{\frac{\tau}{\rho}},$$

where  $\tau$  is the threshold stress of bottom computed using

$$\tau = \frac{g\rho n_b^2 v |v|}{h^{1/3}}. \quad (8)$$

In (7),  $s$  is the submerged specific gravity of sediment given by

$$s = \frac{\rho_s}{\rho_w} - 1.$$

In the present study, we are interested in developing a robust analysis of stresses on the beds generated by sediment transport. There are different models for describing the bed deformation, due to its complex nature only few theoretical models exist which use idealized and simplified assumptions. Most of the deformation models, which are used in practice, are static and usually only work in particular context with no sediment transport included in their formulations and for this reason there is not yet a universally accepted theory of stress analysis by sediment transport. However, we can in general describe the stress distribution in the erodible bed through two processes. The sediment can move in a layer close to the bottom topography which is known as bed load and is characterized by a rolling and sliding movement, or the flow can cause the sediment to separate completely from the bottom in which case it is referred to as suspended load and in this case the sediment is transported as a concentration of the water column and will later be deposited in the bottom.

Let us consider a two-dimensional bed domain  $\Omega$  with smooth boundary  $\partial\Omega$ , the equilibrium governing equations of linear elasticity read [2]

$$\begin{aligned} \frac{\partial\sigma_x}{\partial x} + \frac{\partial\tau_{xz}}{\partial z} &= f_x, \\ \frac{\partial\sigma_z}{\partial z} + \frac{\partial\tau_{xz}}{\partial x} &= f_z, \end{aligned} \quad (9)$$

where  $\sigma_x$  and  $\sigma_z$  are the normal stresses in the  $x$ - and  $z$ -direction, respectively. Here,  $\tau_{xz}$  is the shear stress,  $f_x$  and  $f_z$  are the external forces in the  $x$ - and  $z$ -direction, respectively. The displacement vector is denoted by  $\mathbf{u} = (u_x, u_z)^\top$  and the infinitesimal strain tensor is defined by

$$\epsilon = \frac{1}{2} \left( \nabla \mathbf{u} + (\nabla \mathbf{u})^\top \right). \quad (10)$$

The system has been solved subjected to the following boundary conditions

$$\begin{aligned}\boldsymbol{\sigma} &= \boldsymbol{\sigma}_s, & \text{on } \Gamma_i, \\ \mathbf{u} &= \mathbf{0}, & \text{on } \Gamma,\end{aligned}\tag{11}$$

where  $\boldsymbol{\sigma}_s$  is the sediment stress on the interfacial boundary  $\Gamma_i$ . In the current study, the constitutive relation is defined as

$$\boldsymbol{\sigma} = \mathbf{D} \boldsymbol{\epsilon},\tag{12}$$

where the stress vector  $\boldsymbol{\sigma}$  and the constitutive matrix  $\mathbf{D}$  are given as

$$\boldsymbol{\sigma} = \begin{pmatrix} \sigma_x \\ \sigma_z \\ \tau_{xz} \end{pmatrix}, \quad \mathbf{D} = \frac{E}{(1+\nu)(1-2\nu)} \begin{pmatrix} 1-\nu & \nu & 0 \\ \nu & 1-\nu & 0 \\ 0 & 0 & \frac{1-2\nu}{2} \end{pmatrix},$$

with  $E$  is the Young modulus and  $\nu$  is the Poisson ratio characterizing the bed material. Note that other constitutive relations in (12) can also be applied in the proposed stress analysis in hydro-sediment-morphodynamic without major modifications in our formulation. It should also be stressed that although the equations (9) are static, the interface boundary  $\Gamma_i$  between the water and bed depends on time.

### 3 A coupled finite element/finite volume method

To solve the equations for the considered hydro-sediment-morphodynamic model we proposed a coupled finite element/finite volume method for which transfer conditions are transmitted at the interface  $\Gamma_i$ . A well-balanced one-dimensional finite volume method is used for the sediment transport equations whereas an unstructured two-dimensional finite element method is used for the elasticity equations. Coupling conditions at the interface are also discussed in this section.

#### 3.1 Well-balanced finite volume solution of sediment transport

For the time integration of the system (1) we divide the time interval into sub-intervals  $[t_n, t_{n+1}]$  with variable size  $\Delta t_n$  such that  $t_n = t_{n-1} + \Delta t_n$ ,  $n = 1, 2, \dots$  and  $t_0 = 0$ . We use the notation  $\mathbf{q}^n(x)$  to denote the discrete solution  $\mathbf{q}(t_n, x)$ . In the current work, we use the splitting operator to deal with the differential source terms  $\mathbf{Q}(\mathbf{q})$  and the non-differential source term  $\mathbf{S}(\mathbf{q})$  in (1). The splitting procedure consists of the following two steps:

Step 1: Solve for  $\tilde{\mathbf{q}}$

$$\frac{\tilde{\mathbf{q}} - \mathbf{q}^n}{\Delta t_n} + \frac{\partial \mathbf{F}(\mathbf{q}^n)}{\partial x} = \mathbf{Q}(\mathbf{q}^n).\tag{13}$$

Step 2: Solve for  $\mathbf{q}^{n+1}$

$$\frac{\mathbf{q}^{n+1} - \tilde{\mathbf{q}}}{\Delta t_n} = \mathbf{S}(\tilde{\mathbf{q}}). \quad (14)$$

For the space discretization we discretize the one-dimensional space domain in non-uniform control volumes  $[x_{i-\frac{1}{2}}, x_{i+\frac{1}{2}}]$  with length  $\Delta x_i$  and we use the notation  $\mathbf{q}_i^n$  to denote the space-averaged of  $\mathbf{q} = \mathbf{q}(t, x)$  in the cell  $[x_{i-\frac{1}{2}}, x_{i+\frac{1}{2}}]$  at time  $t_n$ , and  $\mathbf{q}_{i+\frac{1}{2}}^n$  are the intermediate solutions at  $x_{i+\frac{1}{2}}$  at time  $t_n$ ,

$$\mathbf{q}_i^n = \frac{1}{\Delta x_i} \int_{x_{i-\frac{1}{2}}}^{x_{i+\frac{1}{2}}} \mathbf{q}(t_n, x) dx, \quad \mathbf{q}_{i+\frac{1}{2}}^n = \mathbf{q}\left(t_n, x_{i+\frac{1}{2}}\right).$$

Integrating the system (13) over the space-time control domain  $[x_{i-\frac{1}{2}}, x_{i+\frac{1}{2}}] \times [t_n, t_{n+1}]$ , one obtains the following fully discrete system

$$\mathbf{q}_i^{n+1} = \mathbf{q}_i - \frac{\Delta t_n}{\Delta x_i} \left( \mathbf{F}_{i+\frac{1}{2}}^n - \mathbf{F}_{i-\frac{1}{2}}^n \right) + \Delta t_n \mathbf{Q}_i^n, \quad (15)$$

where  $\mathbf{F}_{i\pm\frac{1}{2}}^n = \mathbf{F}(\mathbf{q}_{i\pm\frac{1}{2}}^n)$  are the numerical fluxes at  $x = x_{i\pm\frac{1}{2}}$  and time  $t = t_n$ , and  $\mathbf{Q}_i^n$  is the space-averaged of the source term  $\mathbf{Q}$  defined as

$$\mathbf{Q}_i^n = \frac{1}{\Delta x_i} \int_{x_{i-\frac{1}{2}}}^{x_{i+\frac{1}{2}}} \mathbf{Q}(\mathbf{q}) dx. \quad (16)$$

The spatial discretization (15) is complete when the numerical fluxes  $\mathbf{F}_{i\pm\frac{1}{2}}^n$  and the source term  $\mathbf{Q}_i^n$  are reconstructed. Generally, this step can be carried out using any finite volume method developed in the literature for solving hyperbolic systems of conservation laws, see for example [2]. In the present study, we consider the Roe reconstruction defined as

$$\mathbf{F}_{i+\frac{1}{2}}^n = \frac{1}{2} \left( \mathbf{F}(\hat{\mathbf{q}}_{i+1}^n) + \mathbf{F}(\hat{\mathbf{q}}_i^n) \right) + \frac{1}{2} \mathbf{A} \left( \hat{\mathbf{q}}_{i+\frac{1}{2}}^n \right) \left( \hat{\mathbf{q}}_i^n - \hat{\mathbf{q}}_{i+1}^n \right), \quad (17)$$

where the averaged state  $\hat{\mathbf{q}}_{i+\frac{1}{2}}^n$  is calculated as

$$\hat{\mathbf{q}}_{i+\frac{1}{2}}^n = \begin{pmatrix} \frac{h_i^n + h_{i+1}^n}{2} \\ \frac{\sqrt{h_i^n} u_i^n + \sqrt{h_{i+1}^n} u_{i+1}^n}{\sqrt{h_i^n} + \sqrt{h_{i+1}^n}} \\ \frac{\sqrt{h_i^n} c_i^n + \sqrt{h_{i+1}^n} c_{i+1}^n}{\sqrt{h_i^n} + \sqrt{h_{i+1}^n}} \\ \frac{Z_i^n + Z_{i+1}^n}{2} \end{pmatrix}, \quad (18)$$

and the Roe matrix in (17) is defined as  $\mathbf{A} = \mathbf{R}\mathbf{A}\mathbf{R}^{-1}$  with

$$\mathbf{R} = \begin{pmatrix} 1 & 1 & 1 & 1 \\ \hat{u} & \hat{\lambda}_2 & \hat{\lambda}_3 & \hat{\lambda}_4 \\ \hat{c} - \frac{2\hat{\rho}}{(\rho_s - \rho_w)} & \hat{c} & \hat{c} & \hat{c} \\ 0 & \frac{(\hat{\lambda}_2 - \hat{u})^2 - g\hat{h}}{g\hat{h}} & \frac{(\hat{\lambda}_3 - \hat{u})^2 - g\hat{h}}{g\hat{h}} & \frac{(\hat{\lambda}_4 - \hat{u})^2 - g\hat{h}}{g\hat{h}} \end{pmatrix}, \quad (19)$$

$$\mathbf{A} = \begin{pmatrix} \hat{\lambda}_1 & 0 & 0 & 0 \\ 0 & \hat{\lambda}_2 & 0 & 0 \\ 0 & 0 & \hat{\lambda}_3 & 0 \\ 0 & 0 & 0 & \hat{\lambda}_3 \end{pmatrix},$$

with the four eigenvalues

$$\begin{aligned} \lambda_1 &= u, & \lambda_2 &= 2\sqrt{-Q} \cos\left(\frac{1}{3}\theta\right) + \frac{2}{3}u, \\ \lambda_3 &= 2\sqrt{-Q} \cos\left(\frac{1}{3}(\theta + 2\pi)\right) + \frac{2}{3}u, \\ \lambda_4 &= 2\sqrt{-Q} \cos\left(\frac{1}{3}(\theta + 4\pi)\right) + \frac{2}{3}u, \end{aligned} \quad (20)$$

where  $\theta = \arccos\left(\frac{R}{\sqrt{-Q^3}}\right)$ , with

$$Q = -\frac{1}{9}(u^2 + 3g(h + h\xi)), \quad R = \frac{u}{54}(9g(2h - h\xi) - 2u^2).$$

For the discretization of the source term  $\mathbf{Q}_i^n$  we implement a well-balanced reconstruction investigated in [2]. Thus, the well-balanced discretization of  $\mathbf{Q}_i^n$  is achieved by in splitting the integral in (16) over the two sub-cells  $[x_{i-\frac{1}{2}}, x_i]$  and  $[x_i, x_{i+\frac{1}{2}}]$  of the control volume  $[x_{i-\frac{1}{2}}, x_{i+\frac{1}{2}}]$  as

$$\mathbf{Q}_i^n = \frac{1}{\Delta x_i} \left( \frac{(x_i - x_{i-1})}{2} \mathbf{Q}_{i-\frac{1}{2}}^L + \frac{(x_{i+1} - x_i)}{2} \mathbf{Q}_{i+\frac{1}{2}}^R \right), \quad (21)$$

where  $\mathbf{Q}_{i-\frac{1}{2}}^L$  and  $\mathbf{Q}_{i+\frac{1}{2}}^R$  are the space-averaged of the source term  $\mathbf{Q}$  in the sub-cells  $[x_{i-\frac{1}{2}}, x_i]$  and  $[x_i, x_{i+\frac{1}{2}}]$  defined as

$$\mathbf{Q}_{i-\frac{1}{2}}^L = \begin{pmatrix} 0 \\ -g \frac{h_i + h_{i-1}}{2} (Z_i - Z_{i-1}) \\ 0 \\ 0 \end{pmatrix}, \quad \mathbf{Q}_{i+\frac{1}{2}}^R = \begin{pmatrix} 0 \\ -g \frac{h_{i+1} + h_i}{2} (Z_{i+1} - Z_i) \\ 0 \\ 0 \end{pmatrix}.$$

It is evident that for small water depths, the bed friction term dominates the other terms in the momentum equation. This is mainly due to the presence of the term  $h^{\frac{4}{3}}$  in the dominator of  $\tau$  in (8). To overcome this drawback we use a semi-implicit time integration of the source term  $\mathbf{S}$  in (14) as

$$\begin{aligned} \frac{h^{n+1} - \tilde{h}}{\Delta t_n} &= 0, \\ \frac{(hv)^{n+1} - (\tilde{h}\tilde{v})}{\Delta t_n} &= -gn_b^2 \frac{(hv)^{n+1} |\tilde{v}|}{(\tilde{h})^{\frac{4}{3}}}, \end{aligned} \quad (22)$$

where  $\tilde{h}$  and  $\tilde{v}$  are the water height and velocity obtained from the first step (13) of the splitting procedure. Solving the second equation in (22) for  $(hv)^{n+1}$  yields

$$(hv)^{n+1} = \frac{(\tilde{h}\tilde{v})}{1 + \Delta t_n gn_b^2 |\tilde{v}| / (\tilde{h})^{\frac{4}{3}}}. \quad (23)$$

As in most explicit time integration schemes, the time step in our finite volume method is selected using a Courant-Friedrichs-Lewy (CFL) condition. In our simulations, the Courant number  $Cr$  is fixed and  $\Delta t_n$  is chosen at each time step according to the following CFL condition

$$\Delta t_n = Cr \frac{\min_i(\Delta x_i)}{\max_{k=1,2,3,4} \left( |\hat{\lambda}_k^+|, |\hat{\lambda}_k^-| \right)}, \quad (24)$$

where  $\hat{\lambda}_k^\pm$  are the eigenvalues (20) computed using the space-averaged solutions in the control volume  $[x_{i-\frac{1}{2}}, x_{i+\frac{1}{2}}]$  and its two neighbouring cells.

### 3.2 Unstructured finite element solution of elasticity

The starting point for the finite element method is the variational formulation of the strain energy in the domain  $\Omega$ . Thus, multiplying the strong form of  $x$ -direction equation in (9) by an arbitrary weight function  $\phi_x$  and integrate over the domain yields

$$\int_{\Omega} \frac{\partial \sigma_x}{\partial x} \phi_x \, d\mathbf{x} + \int_{\Omega} \frac{\partial \tau_{xz}}{\partial z} \phi_x \, d\mathbf{x} - \int_{\Omega} f_x \phi_x \, d\mathbf{x} = 0.$$

Using the Green-Gauss theorem, the above equation becomes

$$\oint_{\partial\Omega} \sigma_x n_x \phi_x \, d\mathbf{x} - \int_{\Omega} \frac{\partial \phi_x}{\partial x} \sigma_x \, d\mathbf{x} + \oint_{\partial\Omega} \tau_{xz} n_z \phi_x \, d\mathbf{x} - \int_{\Omega} \frac{\partial \phi_x}{\partial z} \tau_{xz} \, d\mathbf{x} - \int_{\Omega} f_x \phi_x \, d\mathbf{x} = 0,$$

where  $\mathbf{x} = (x, z)^\top$  and  $\mathbf{n} = (n_x, n_z)^\top$  is the outward unit normal on  $\partial\Omega$  with  $\partial\Omega = \Gamma \cup \Gamma_i$ . Using the  $x$ -component of the traction  $\mathcal{T}_x = \sigma_x n_x + \tau_{xz} n_z$ , the above equation can be written as

$$\oint_{\partial\Omega} \mathcal{T}_x \phi_x \, d\mathbf{x} - \int_{\Omega} \left( \frac{\partial \phi_x}{\partial x} \sigma_x + \frac{\partial \phi_x}{\partial z} \tau_{xz} \right) \, d\mathbf{x} - \int_{\Omega} f_x \phi_x \, d\mathbf{x} = 0. \quad (25)$$

Similar steps applied to the  $z$ -direction equation in (9) give

$$\oint_{\partial\Omega} \mathcal{T}_z \phi_z \, d\mathbf{x} - \int_{\Omega} \left( \frac{\partial \phi_z}{\partial x} \tau_{xz} + \frac{\partial \phi_z}{\partial z} \sigma_z \right) \, d\mathbf{x} - \int_{\Omega} f_z \phi_z \, d\mathbf{x} = 0, \quad (26)$$

where  $\mathcal{T}_z = \sigma_z n_z + \tau_{xz} n_x$ . Adding the two equations (25) and (26) yields

$$\begin{aligned} \oint_{\partial\Omega} (\mathcal{T}_x \phi_x + \mathcal{T}_z \phi_z) \, d\mathbf{x} - \int_{\Omega} (f_x \phi_x + f_z \phi_z) \, d\mathbf{x} - \\ \int_{\Omega} \left( \frac{\partial \phi_x}{\partial x} \sigma_x + \frac{\partial \phi_x}{\partial z} \tau_{xz} + \frac{\partial \phi_z}{\partial z} \sigma_z + \frac{\partial \phi_z}{\partial x} \tau_{xz} \right) \, d\mathbf{x} = 0, \end{aligned}$$

which can be reformulated in a vector form as

$$\int_{\Omega} \hat{\boldsymbol{\phi}} \cdot \boldsymbol{\sigma} \, d\mathbf{x} = \oint_{\partial\Omega} \boldsymbol{\phi}^\top \cdot \boldsymbol{\mathcal{T}} \, d\mathbf{x} + \int_{\Omega} \boldsymbol{\phi}^\top \cdot \mathbf{f} \, d\mathbf{x}, \quad (27)$$

where  $\boldsymbol{\phi} = (\phi_x, \phi_z)^\top$ ,  $\boldsymbol{\mathcal{T}} = (\mathcal{T}_x, \mathcal{T}_z)^\top$  and  $\hat{\boldsymbol{\phi}} = \left( \frac{\partial \phi_x}{\partial x}, \frac{\partial \phi_z}{\partial z}, \frac{\partial \phi_x}{\partial z} + \frac{\partial \phi_z}{\partial x} \right)^\top$ . To solve the weak form (27) with the finite element method, the domain  $\Omega$  is discretized into a set of elements where the solution is approximated in terms of the nodal values  $U_j$  and the polynomial basis functions  $N_j(x, z)$  as

$$\mathbf{u}(x, z) = \sum_{j=1}^{N_d} \mathbf{U}_j N_j(x, z), \quad (28)$$

where  $N_d$  is the number of mesh nodes. In the present work, we consider quadratic triangular elements with six nodes for which the elementary matrices are assembled into a global system of equations

$$\mathbf{K}\mathbf{u} = \mathbf{b}, \quad (29)$$

where  $\mathbf{K}$  is the global stiffness matrix,  $\mathbf{u}$  is the nodal displacement vector and  $\mathbf{b}$  is the force vector. In our simulations, the matrix  $\mathbf{K}$  is decomposed into an  $LUL^\top$  factorization, then the solution is reduced to backward/forward substitutions after updating the right-hand side vector  $\mathbf{b}$  at every time step.

### 3.3 Implementation of coupling conditions at the interface

One of the advantages in using non-uniform grids in the finite volume solution is to avoid interpolations at the interface for interchange coupling conditions.

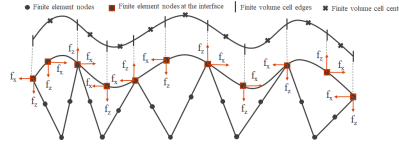


**Fig. 1.** An illustration of finite element and finite volume nodes at the interface.

Here, the selected control volumes in the finite volume methods coincide with the finite element nodes on the interface as shown in Figure 1. At each time step coupling conditions are transferred on the interface for both models to update the solutions for the displacement  $\mathbf{u}$ , water height  $h$  and water velocity  $v$ . In the present work, the deformed finite element nodes on the interface are used to reconstruct the bed  $Z(x, t)$  for the shallow water equations (1). Here, a triangular finite element with three nodes on the interface yields two non-uniform control volumes the edges of which are the three nodes and their centers are obtained by averaging the coordinates of these nodes, compare Figure 1. We also assume that once the deformation occurs, the time variation in these coordinates is negligible and therefore no need for interpolation procedures to reconstruct the bed topography in the finite volume method. This bed profile is used in the finite volume solution of the flow system to obtain the water height  $h^{n+1}$  and the water velocity  $v^{n+1}$  at the next time level  $t_{n+1}$ . For coupling conditions from the water flow to the bed on the interface, the forces  $f_x$  and  $f_z$  in the elasticity equations (9) are reconstructed at each time step. Here, the horizontal force  $f_x$  in the  $x$ -direction is updated using the friction term as

$$f_x = -gn_b^2 h^{n+1} \frac{v^{n+1} |v^{n+1}|}{(h^{n+1})^{\frac{4}{3}}}. \quad (30)$$

The vertical force  $f_z$  in the  $z$ -direction is reconstructed at each time step using the change in the hydrostatic pressure as

$$p^{n+1} = -\rho g \frac{h^{n+1} - h^n}{\Delta t}_n,$$

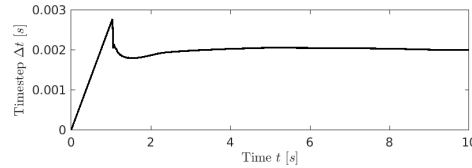
and at each node of the three finite element nodes located on the interface, the force  $f_z$  is distributed using the integral form as

$$\begin{aligned} f_z^{(1)} &= \int_{-1}^1 -\frac{1}{2}\xi(1-\xi)p^{n+1}\frac{\bar{h}}{2}d\xi = \frac{1}{6}p^{n+1}\bar{h}, \\ f_z^{(2)} &= \int_{-1}^1 (1-\xi^2)p^{n+1}\frac{\bar{h}}{2}d\xi = \frac{2}{3}p^{n+1}\bar{h}, \\ f_z^{(3)} &= \int_{-1}^1 \frac{1}{2}\xi(1+\xi)p^{n+1}\frac{\bar{h}}{2}d\xi = \frac{1}{6}p^{n+1}\bar{h}, \end{aligned} \quad (31)$$

where  $\bar{h}$  is the edge length of the considered element on the interface. It is easy to verify that  $f_z^{(1)} + f_z^{(2)} + f_z^{(3)} = p^{n+1}\bar{h}$ . The total force  $f_z$  in the  $z$ -direction

**Table 1.** Parameters used in simulations for the dam-break problem.

Quantity	Reference value	Quantity	Reference value
$\rho_w$	1000 $kg/m^3$	$\nu$	$1.2 \times 10^{-6} m^2/s$
$\rho_s$	2650 $kg/m^3$	$n_b$	0.03 $s/m^{1/3}$
$g$	9.81 $m/s^2$	$p$	0.4
$\varphi$	0.015 $m^{1.2}$	$\theta_c$	0.045

**Fig. 2.** Time evolution of the time step  $\Delta t$  using the CFL condition (24).

is obtained by accumulating the elemental forces on the overlapping nodes, see Figure 1 for an illustration.

## 4 Numerical results

We solve the problem of a dam-break over erodible bed studied in [3] using the parameters listed in Table 1. All the simulations are performed using a mesh with 100 gridpoints (unless stated) and numerical results are displayed at time  $t = 10 \text{ min}$  using a time step adjusted according to the CFL condition (24) with  $Cr = 0.75$ . The obtained time evolution of the time step  $\Delta t$  is presented in Figure 2 confirming that it does not overpass  $3 \times 10^{-3}$  for this problem. Figure 3 depicts the mesh used in our simulations before and after deformation. Based on a mesh convergence study not reported here for brevity, an unstructured triangular mesh with 1749 quadratic elements and 3763 nodes is used in our simulations as it offers a compromise between accuracy and efficiency in the numerical method.

To validate our results to experiment data for this example, we present in Figure 4 the results obtained at time  $t = 10$ . The agreement between the numerical simulations and experimental measurements in this figure is fairly good. The water free-surface and the erodible bed are well predicted by the proposed numerical approach. Obviously, the computed results for both water height and bed profile verify the stability and the shock capturing properties of the numerical method for this dam-break problem over a wet bed. Figure 5 depicts the distribution of the normal stress component  $\sigma_z$  and the shear stress  $\tau_{xz}$ . It is clear that maximum values of stresses are located on the bed surface where the erosion has taken place. The deformed bed has also been accurately resolved using our finite element method. Under the considered conditions, stress dis-

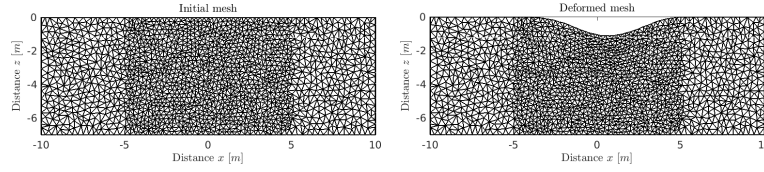


**Fig. 3.** Initial mesh (left) and deformed mesh at time  $t = 10$  s (right).

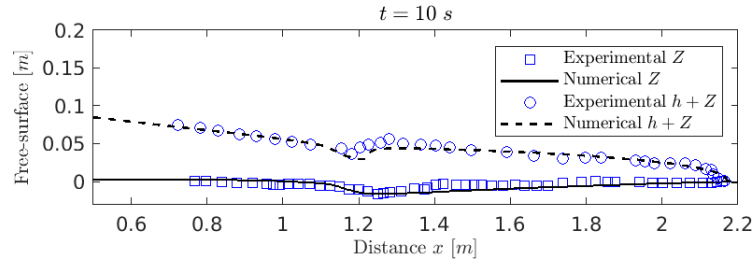


**Fig. 4.** Comparison between the numerical results and experiments at time  $t = 10$  s.

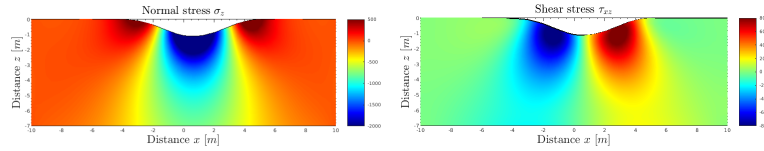


**Fig. 5.** Normal stress  $\sigma_z$  (left) and shear stress  $\tau_{xz}$  at time  $t = 10$  s (right).

tributions exhibit symmetrical features in both stresses. Furthermore, no mesh distortion has been detected in all results obtained for this dam-break problem. It should be stressed that results from the proposed coupled model should be compared with observations of laboratory free-surface flows and bed deformations for this problem. However, as of now, no data is available to carry out this comparison study. Thus, at the moment we can only perform numerical simulations and verify that results are plausible and consistent.

## 5 Concluding remarks

An accurate and efficient computational algorithm is presented in this study for stress analysis in hydro-sediment-morphodynamic models. The linear elasticity equations for the bed topography are coupled to the shallow water hydro-sediment-morphodynamic equations to form a consistent model for the considered problems. At the bed interface between the water surface and the bedload, transfer conditions are also developed using frictional forces and hydrostatic

pressures. As a numerical solver we implement a hybrid finite volume/finite element method. The method is well-balanced for solutions of the shallow water equations and uses quadratic elements on unstructured meshes for the elasticity equations. Numerical results are presented for the problem of a dam-break over erodible bed and the computed solutions demonstrated the ability of the proposed model to accurately capture the stress distributions for erosional and depositional deformations.

## References

1. Aguirre, J., Castro, M., Luna, T.: A robust model for rapidly varying flows over movable bottom with suspended and bedload transport: Modelling and numerical approach. *Advances in water resources* **140**, 1–22 (2020)
2. Al-Ghosoun, A., Osman, A., Seaid, M.: A computational model for simulation of shallow water waves by elastic deformations in the topography. *Communications in Computational Physics* **29**, 1095–1124 (2021)
3. Benkhaldoun, F., Sari, S., Seaid, M.: A flux-limiter method for dam-break flows over erodible sediment beds. *Applied Mathematical Modelling* **36**(10), 4847–4861 (2012)
4. Cao, Z., Pender, G., Wallis, S., Carling, P.: Computational dam-break hydraulics over erodible sediment bed. *Journal of hydraulic engineering* **130**(7), 689–703 (2004)
5. Engelund, F., Hansen, E.: Monograph on sediment transport in Alluvial streams TUDelf. *The Northernlands* **37**, 1–14 (1997)
6. Escalante, C., Luna, T., Castro, M.: Non-hydrostatic pressure shallow flows: GPU implementation using finite volume and finite difference scheme. *International Journal of computer-aided engineering and software* **338**, 631–659 (2018)
7. Grabowski, R.: Measuring the shear strength of cohesive sediment in the field. *Geomorphological techniques* **3**, 1–7 (2014)
8. Grass, A.: Sediment transport by waves and currents. Technical Report FL29, SERC. London Cent. Mar (1981)
9. Hairsine, B., Rose, W.: Modelling water erosion due to overland flow using physical principles. *Water resources* **28**, 237–243 (1992)
10. Hajigholizadeh, M., Melesse, A., Fuentes, H.: Erosion and sediment transport modelling in shallow waters: A review on approaches, models and applications. *International Journal of environmental research and public health* **15**, 1–24 (2018)
11. Hazelden, J., Boorman, A.: Soils and managed retreat in south east england. *Soil use and management* **30**, 180–189 (2001)
12. Merritt, S., Letcher, A., Jakeman, J.: A review of erosion and sediment transport models. *Environmental model software* **18**, 761–799 (2003)
13. Merritt, W., Letcher, R., Jakeman, A.: A review of erosion and sediment transport models. *Environment modelling and software* **18**, 761–799 (2003)
14. Recanatesi, F., Ripa, A., Leoni, M.: Assessment of software runoff management practices and PMPs under soil sealing: A study case in a peri-urban watershed of the metropolitan area of Rome. *J. Environ. Manag* **201**, 6–18 (2017)
15. Reisinger, A., Gibeaut, J., Tissot, P.: Estuarine suspended sediment dynamics: observations derived from over a decade of Satellite data. *Frontiers in marine science* **4**, 1–10 (2017)
16. Takken, I., Govers, V., Nachtergaele, G., Steegen, J.: The effect of tillage-induced roughness on runoff and erosion patterns. *Geomorphology* **37**, 1–14 (2001)